A Filter Theory Approach to the Synthesis of Capacitive Power Transfer Systems

Masoud Ahmadi, *Student Member, IEEE*, Loïc Markley, *Senior Member, IEEE*, and Thomas Johnson, *Member, IEEE*

***Abstract*— Resonant-coupled wireless power transfer (WPT) systems are typically modeled as circuits with inductively or capacitively coupled resonators. In a two-resonator system, the transmit and receive resonators are linked by a coupling coefficient, and the coupling can be adjusted for critical coupling, overcoupling, and undercoupling. In this work, we show that the coupled-resonator structure is equivalent to a filter structure and provide a demonstration of how filter theory can be used to design a capacitive WPT system. An advantage of this approach is that it provides access to a wide range of canonical structures and methods of impedance scaling to realize matched links. We show a maximally flat filter has a critically coupled response and an equiripple Chebychev filter has an overcoupled response. There is a relationship between frequency bandwidth in a filter design and spatial bandwidth in a WPT link. Therefore, the filter context can be used to synthesize wideband filters that are more robust to spatial variation than narrowband filters.**

***Index Terms*— Capacitive power transfer (CPT), filter, inductive power transfer (IPT), inverter, wireless power transfer (WPT).**

I. Introduction

With the proliferation of battery-powered electronic devices, the demand for automated, convenient, fast, and safe charging solutions is greater than ever. Research into near-field wireless power transfer (WPT) systems has been rapidly growing as a way to enable convenient charging that removes the need to physically connect a cable to charge the device. With WPT systems, the power connector can be removed, and the device can be completely sealed. Applications include wearable electronics [1], implantable medical devices [2], [3], sensor networks [4], and electric vehicle charging [5]–[7].

In a near-field WPT system, energy is coupled between a transmitter and a receiver using an electromagnetic field. The field is primarily reactive and radiative losses should be minimized. Resonators are usually employed to enable efficient electromagnetic coupling across an air gap between the transmitter and the receiver. In the near field, the electromagnetic coupling between the resonators may be dominated by the magnetic field [8], the electric field [9], or a combination of both [10]. If the magnetic field coupling is dominant, the WPT system is called an inductive power transfer (IPT) system. Conversely, if the electric field coupling is dominant, the system is called a capacitive power transfer (CPT) system.

Since WPT systems consist of coupled resonators, they are structurally similar to coupled-resonator bandpass filters that are designed using a filter theory. For example, bandpass filters are often implemented by transforming canonical prototypes into structures consisting of coupled resonators. In this article, we show that the similarities between these coupled-resonator structures enable us to apply filter synthesis methods to the design of WPT systems. Specifically, we focus on the synthesis of matched CPT resonators.

The design of compensation networks that maximize the efficient delivery of real power to a load through a reactive coupling link usually employs direct circuit analysis techniques for specific network topologies. The compensation circuits can consist of structures composed of L-network [11]–[13], Π-network [14], T-network sections [15], [16], inverters [17], [18], and cascades of different combinations of these types of networks [19], [20]. Also, the analysis and design of compensation networks usually focus on a single frequency.

Filter theory offers a distinctly different approach to the synthesis of matched CPT links that exploit the wide range of well-known canonical filter prototypes offering a diverse range of frequency response characteristics. The filter synthesis approach includes access to tabulated values of normalized coefficients for specific frequency response and specific termination resistances. The values of circuit elements are easily found from the well-known filter design equations, and filter theory has a wide range of circuit topologies. We show that the maximally flat frequency response (Butterworth) is equivalent to critical coupling in CPT and filters with equiripple frequency responses (Chebyshev) are equivalent to overcoupled CPT systems. Therefore, filter theory provides a general, systematic, and diverse range of canonical network structures that can be matched for specific terminal impedances using design tables for specific frequency response characteristics.

Manuscript received March 31, 2020; revised June 9, 2020; accepted July 7, 2020. Date of publication July 20, 2020; date of current version February 3, 2022. This work was supported in part by the Natural Sciences and Engineering Research Council of Canada (NSERC), in part by the Canada Foundation for Innovation (CFI), in part by the British Columbia Knowledge Development Fund (BCKDF), and in part by the National Research Council (NRC). Recommended for publication by Associate Editor Dehong M. Xu. *(Corresponding author: Masoud Ahmadi.)*

The authors are with the School of Engineering, The University of British Columbia, Kelowna, BC V1V 1V7, Canada (e-mail: masoud.ahmadi@alumni.ubc.ca; loic.markley@ubc.ca; thomas.johnson@ubc.ca).

Color versions of one or more of the figures in this article are available online at https://ieeexplore.ieee.org.

Digital Object Identifier 10.1109/JESTPE.2020.3010424

Filter theory also offers other insights into the synthesis of WPT systems. For example, although WPT systems are inherently narrowband, they need to be robust in terms of spatial bandwidth since reactance varies with spatial changes. In a filter design, reactance variation as a function of frequency is controlled, and as shown in Section V-C, there are relationships between the spatial and frequency bandwidths.

In this article, a synthesis methodology is described, which begins with a capacitance matrix that models the physical conductors in a CPT link. The capacitance matrix is reduced and transformed into an equivalent circuit. Assuming that the physical conductors satisfy a physical symmetry condition, the equivalent circuit can be reduced to a Π-network of capacitances called a half circuit. The half circuit is then transformed into a network that can be matched with a canonical filter network. An important step in the transformation is partitioning the half circuit into a network that consists of an impedance inverter. The synthesis method is demonstrated through six design examples with the Butterworth and Chebychev frequency responses. The impact of finite Q on the overall efficiency of the system is explored, and each design example is verified in the experiment. Design examples of CPT links with different bandwidths are compared in terms of spatial bandwidth, and we show that networks with broad bandwidths can have improved spatial bandwidth.

II. CPT Physical Structures

In this section, we describe the physical geometry of the plates in CPT systems and how an equivalent circuit model is derived. Physical symmetry in the CPT plate geometry can be exploited to simplify the electrostatic simulations used to extract the capacitance matrix. We show that under specific symmetry conditions, the equivalent capacitance circuit for the CPT electrodes can be reduced to a half-circuit model consisting of three capacitances in a Π-network. Once an equivalent half-circuit model is constructed, the filter theory can be applied to synthesized matched networks with predefined frequency characteristics.

A. Four Plate CPT

For the development of relations between filter theory and CPT systems, we consider a four-plate transmission link [21]–[24], as shown in Fig. 1(a). In the four-plate configuration, there are two possible physical planes of symmetry that are useful to distinguish: plane aa' and plane bb'. Symmetry about plane aa' is common in many CPT systems where each pair of plates at the transmitter and receiver is identical. Symmetry about plane bb' applies to four-plate configurations that have transmit and receive plates of the same size. The methods described are applicable to CPT systems that always have symmetry about aa', but they may have asymmetry about bb'. The terms "symmetric" and "asymmetric" are used to identify whether the physical conductors have symmetry about plane bb'.

In all four-plate configurations that have physical symmetry along plane aa', image theory can be used to construct an equivalent two-conductor system. Assuming that the transmitter is driven by a balanced differential source and the receiver is coupled to a balanced load, a virtual ground plane exists along the plane aa'. The virtual ground can be replaced by a perfect electric conducting plane that effectively splits the four-conductor system into two identical half circuits. An equivalent two-conductor half circuit is shown in Fig. 1(b). The two-conductor half circuit can be modeled electrically by three capacitances arranged in a Π-network, as shown in Fig. 1(c). The Π-network capacitances are identified as $C_{\rm TX}$, C_m, and $C_{\rm RX}$. When the physical size of transmit and receive conductors is identical, this leads to a symmetric Π-network where $C_{\rm TX} = C_{\rm RX}$. Otherwise, for different sized transmit and receive plates, the Π-network is asymmetric and $C_{\rm TX} \neq C_{\rm RX}$. We will show through filter theory thatto obtain maximum power transfer, physically symmetric CPT links have equal source and load resistances, while physically asymmetric configurations have unequal source and load resistances.

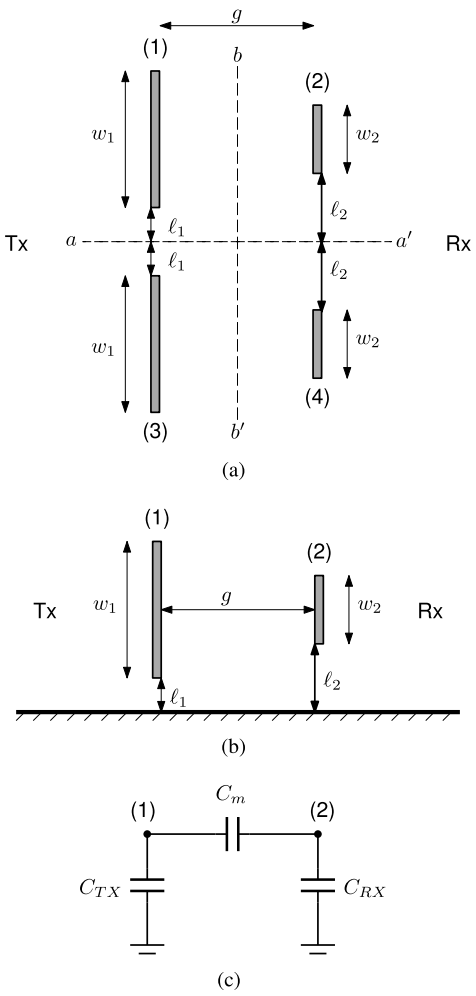

Fig. 1. (a) Four-plate CPT. In general, the size of the transmitter and receiver plates is different. (b) Assuming that the transmitter is fed by a balanced differential source and the receiver is coupled to a balanced load, a virtual ground plane exists along the physical line of symmetry, which simplifies the structure. (c) Equivalent circuit of the physical half circuit.

Although a four-plate CPT is used as an example, multiconductor CPT structures can also be modeled by equivalent

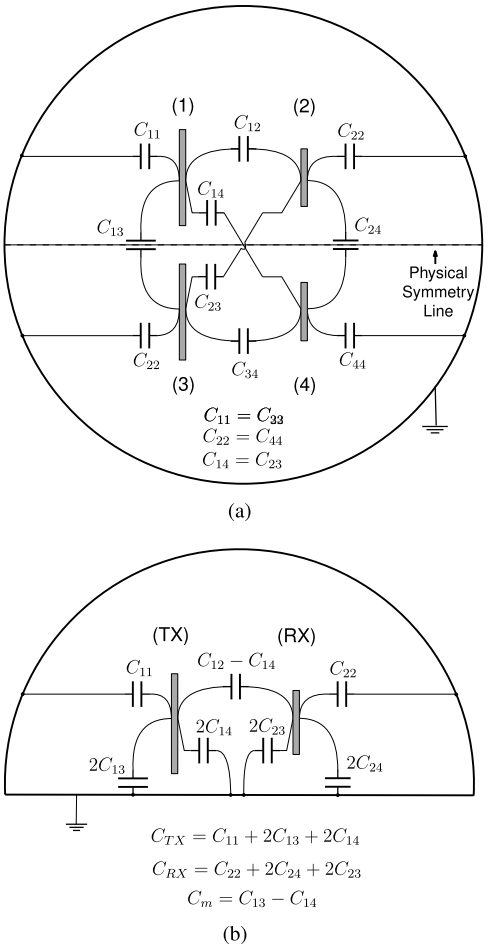

Fig. 2. Electrostatic simulation models annotated with Maxwell capacitances for each electrode. (a) Four-plate CPT configuration illustrating the physical symmetry plane that exists when a balanced source and loads are connected to the transmit and receive plates. (b) Equivalent half-circuit model for the four-plate CPT. Note that since the midpoints of the cross-coupling terms, C_{14} and C_{23}, shown in (a), are not at virtual ground when the transmit and receive plates are not at the same potential, C_{13} must be modified to C_{13} and C_{14} before the physical symmetry plane can be replaced by a ground plane [7], [30].

Π-networks similar to Fig. 1(c) [25], [26]. For example, direct circuit analysis of four- and six-plate CPT systems have been used to synthesize equivalent capacitive Π-networks [27], [28]. Another example is the elegant simplification of a six-plate CPT to a Π-network using physical symmetry and a special feeding mechanism [7]. We show later that once an equivalent capacitive Π-network is found, filter synthesis methods can be used to implement matched CPT links.

B. Electrostatic Models for Finding Circuit Capacitances

Capacitance models of four-plate CPT systems are found through electrostatic simulations of the physical plate geometries. The electrostatic simulations generate capacitance matrices that can be transformed into networks of interelectrode capacitances, as shown in Fig. 2(a). The field simulation consists of the electrodes enclosed in a large conducting sphere that provides a common ground reference for the system. The diameter of the sphere is chosen to be sufficiently large compared with the size of the conductors such that self-capacitances are calculated accurately.

Assuming that the four-plate CPT has physical symmetry, image theory [29] can be used to simplify the system to an equivalent two-plate model, as shown in Fig. 2(b). The image model of the electrodes significantly simplifies the numerical computation of the fields and is used whenever physical symmetry is present in the electrode geometry of the CPT system. Electrostatic simulations of an equivalent two-plate system are made in semispherical domains, and the fields are identical to the fields in the upper semisphere of the symmetric four-plate system.

The field simulation of a two-plate image model yields a two-by-two capacitance matrix that can be directly mapped to the half-circuit model in Fig. 1(c). The equivalent half-circuit capacitances can also be expressed in terms of the capacitance matrix for a full four-plate simulation model. For completeness, the two-plate model shown in Fig. 2(b) is annotated with capacitance equations that are expressed in terms of the original four plate system. The figure also includes expressions for the equivalent half-circuit capacitances C_{TX}, C_{RX}, and C_m.

III. CPT Synthesis From Filter Circuits

In this section, we work through steps to transform a bandpass filter into an equivalent circuit that has two resonators coupled through a capacitive Π-network. The goal of the transformation is to synthesize a matched CPT link that includes a capacitive Π-network that can be directly related to the CPT plate capacitances. When we use a canonical filter prototype for synthesis, the matched CPT link can be designed to have a specific frequency response with known port impedances that deliver maximum load power that is theoretically 100% efficient except for limitations in Q of the components in the network.

The synthesis begins with a canonical lowpass filter prototype circuit that has a known frequency response characteristic. Butterworth filters have a maximally flat-type frequency response, whereas Chebyshev filters have an equi-ripple-type frequency response. Normalized values of the circuit elements are tabulated in filter design tables for low-pass filters with a cutoff frequency of 1 rad/s. The filter order (N) determines the number of reactive elements in the network, and the normalized component values are identified as g_0, g_1, …, g_{N+1}. The value for g_0 is the source resistance or conductance, and the value for g_{N+1} is the load resistance or conductance. Frequency and impedance scaling can then be used to transform the canonical prototype into a bandpass filter by replacing each reactive element with an LC resonator [31].

We begin with the synthesis of a second-order ($N = 2$) lumped element bandpass filter prototype shown in Fig. 3(a). The values for the circuit elements are

$$R_0 = \frac{k_z}{g_0} \quad L_1' = \frac{k_z g_1}{\omega_b} \quad C_1' = \frac{1}{\omega_o^2 L_1'}$$
$$R_3 = k_z g_3 \quad C_2' = \frac{g_2}{k_z \omega_b} \quad L_2' = \frac{1}{\omega_o{}^2 C_2'}. \tag{1}$$

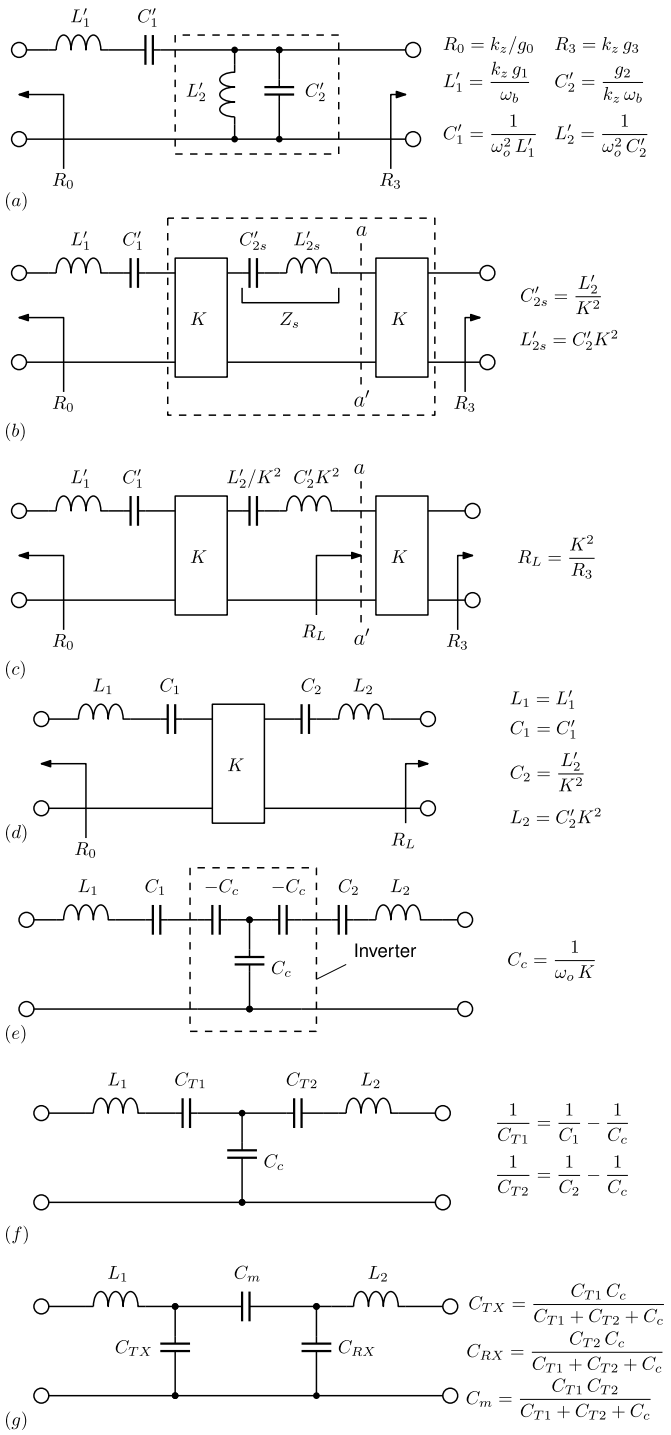

Fig. 3. Summary of steps to transform a second-order bandpass filter prototype into a CPT equivalent circuit model: (a) lumped element bandpass filter prototype; (b) shunt resonator replaced with impedance inverters and series resonator; (c) definition of equivalent load resistance R_L; (d) removal of output inverter; (e) replacement of ideal inverter with equivalent T-network of capacitances; (f) filter with T-network of capacitances; and (g) filter with Π-network of capacitances.

In these equations, k_z is the impedance scaling constant, ω_b is the bandwidth of the filter, and ω_o is the center frequency of the bandpass filter. It is also useful to write expressions in terms of the normalized frequency bandwidth of the filter defined as

$$\Delta = \frac{\omega_b}{\omega_o}. \tag{2}$$

Note that the filter prototypes used in this article are based on nonzero and finite source and load resistances. Filter networks can also be synthesized with ideal voltage or current sources placed at the input [32]; however, these cases are beyond the scope of this article.

The filter is shown in Fig. 3(a) and is comprised of a series resonator (L_1' and C_1') in cascade with a shunt resonator (L_2' and C_2'). Butterworth or Chebyshev filter design tables are used to find the normalized filter values g_n, for $n = 0, 1, 2, 3$, while k_z, ω_b, and ω_o provide the appropriate frequency and impedance transformations. As a side note on notation, primed variables are used to represent the canonical bandpass filter elements, whereas unprimed variables are used to represent the coupled series-resonator elements.

The shunt resonator in Fig. 3(a) is replaced with an equivalent network consisting of a series resonator Z_s' and two impedance inverters with impedance parameter K. The circuit is shown in Fig. 3(b). Similar transformation steps are often done in a microwave filter design [33]. The circuits in the dashed boxes are designed to have the same magnitude response; the phase response may be different depending on how the inverters are implemented.

The transformation of the circuit in Fig. 3(a) into (b) is obtained by matching the z_{11}-parameters for the networks in the dashed boxes. Both networks are symmetric; therefore, $z_{11} = z_{22}$. Since the two networks in Fig. (a) and (b) are equivalent, z_{11} must be the same yielding

$$C_{2s}' = \frac{L_2'}{K^2} \tag{3}$$

and

$$L_{2s}' = C_2'\, K^2. \tag{4}$$

Therefore, the two circuits have the same open-circuit input and output impedances providing (3) and (4) are satisfied.

In the next step, we remove the second inverter (at the output) from the circuit by replacing it with an equivalent load resistance. This step is shown in Fig. 3(c). The impedance seen looking toward the load at plane aa' is R_L where

$$R_L = \frac{K^2}{R_3}. \tag{5}$$

Therefore, the output inverter and the load R_3 can be replaced by R_L as shown in Fig. 3(d).

The next step is to replace the remaining ideal impedance inverter with a physically realizable impedance inverter. There are many well-known realizations of inverters, including T- and Π-networks of capacitors and inductors [33]. For the example shown in Fig. 3(e), a T-network of capacitors is used to implement the impedance inverter. The network consists of two negative series capacitances $-C_c$ and one positive shunt capacitance C_c. The physical inverter is frequency dependent, unlike the ideal inverter, but for relatively narrowband structures, the inverter introduces very small deviations in frequency response.

The series capacitances in Fig. 3(e) can be combined into equivalent capacitances as shown in Fig. 3(f). The equivalent

capacitances are

$$C_{T1} = \frac{C_c C_1}{C_c - C_1} \tag{6a}$$

$$C_{T2} = \frac{C_c C_2}{C_c - C_2}. \tag{6b}$$

From these equations, it is clear that $C_c > \max(C_1, C_2)$ for the system to be physically realizable. As shown by examples later, this condition is easily met for practical designs.

The T-network of capacitances in circuit Fig. 3(f) can be replaced by an equivalent Π-network of capacitances, as shown in Fig. 3(g). Using a Y-Δ transformation, the capacitances in the Π network are

$$C_{\rm TX} = \frac{C_{T1} C_c}{C_{T1} + C_{T2} + C_c} \tag{7a}$$

$$C_{\rm RX} = \frac{C_{T2} C_c}{C_{T1} + C_{T2} + C_c} \tag{7b}$$

$$C_m = \frac{C_{T1} C_{T2}}{C_{T1} + C_{T2} + C_c}. \tag{7c}$$

We have now completed the transformation of the canonical bandpass circuit in Fig. 3(a) into an equivalent circuit (g) that includes a capacitive Π-network, where the Π-network is associated with the physical CPT half circuit shown earlier in Fig. 1(c).

Although it is not evident from the preceding equations, filter theory offers other useful insights with regard to the impedance of the inverter and its relation to the terminal resistances of the filter network. If the Π-network is symmetric ($C_{\rm TX} = C_{\rm RX}$), then the source and load resistances are equal for Butterworth and Chebyshev frequency response characteristics. In addition, under conditions of symmetry, the inverter impedance is also equal to the source and load resistance. Therefore, for a symmetric CPT, $R_s = R_L = K$. For an asymmetric CPT half circuit, where $C_{\rm TX} \neq C_{\rm RX}$, the source and load resistances are unequal.

In summary, the steps in Fig. 3 show how a bandpass filter prototype can be transformed into a network that is equivalent to a CPT link. Knowing these steps, we can reverse the process and work from a physical design of network capacitances and relate it back to a bandpass filter prototype to determine inductor matching components and terminal impedances.

IV. Synthesis of Filters From Geometry

The theory presented in Section III worked through steps to transform a filter structure into an equivalent circuit network that can be related to the physical implementation of a CPT system. Although these design steps shed light on the relationship between filter networks and CPT, a practical application of the theory usually begins with a specific plate geometry that is then matched using circuit networks. Therefore, it very useful to reverse the process in Section III and work from the physical geometry to an equivalent filter network that has specific terminal impedances and bandwidth requirements. The synthesis of matching networks for CPT systems using the filter theory is discussed next.

As shown in Fig. 1, physical CPT structures, such as four-plate systems, can be modeled by an equivalent Π-network of three capacitances. The capacitances can be used to calculate the coupling coefficient K_C that is defined as

$$K_C = \frac{C_m}{\sqrt{(C_{\rm TX} + C_m)(C_{\rm RX} + C_m)}}. \tag{8}$$

In general, $C_{\rm TX}$ is not equal to $C_{\rm RX}$ because the geometry of the transmit and receive plates may be different. An asymmetry parameter is useful for analytic expressions, and the parameter is defined as

$$m = \frac{C_{\rm RX} + C_m}{C_{\rm TX} + C_m}. \tag{9}$$

Using the asymmetry parameter, the coupling coefficient in (8) is

$$K_C = \frac{1}{\sqrt{m}} \frac{C_m}{C_{\rm TX} + C_m}. \tag{10}$$

When $m = 1$, the CPT link is symmetric between the transmit and receive ports, and when $m \neq 1$, the link is asymmetric. The asymmetry parameter m is also fundamentally linked with the bandpass filter design theory in Fig. 3. The parameter m is the scaling factor relating the two series resonators in Fig. 2(d) such that

$$C_2 = mC_1 \tag{11a}$$

$$L_2 = L_1/m. \tag{11b}$$

We can also express the coupling coefficient in terms of the filter prototype parameters in Section III and show that

$$K_C = \frac{\Delta}{\sqrt{g_1 g_2}} \tag{12}$$

where Δ is the relative bandwidth of the filter defined in (2). The equation shows how the bandwidth of the filter network relates to the coupling coefficient: a weakly coupled network is narrowband and a tightly coupled network is broadband. The coupling coefficient also depends on the choice of the canonical filter circuit elements g_1 and g_2. These element values are, in turn, related to the frequency response of the filter. Later, it will be shown that filter coefficient values selected for Butterworth (maximally flat) frequency responses correspond to critically coupled CPT links, whereas Chebyshev coefficients correspond to overcoupled CPT links.

Next, we develop a set of design equations that can be applied to the synthesis of matched CPT links using the filter theory. The transformation steps are summarized in Fig. 4. In the first step, the capacitive Π-network is transformed to an equivalent T-network using a Y-Δ transformation. The T-network capacitances are

$$C_{T1} = \frac{C_{\rm TX} C_m}{C_{\rm sum}} \tag{13a}$$

$$C_c = \frac{C_{\rm TX} C_{\rm RX}}{C_{\rm sum}} \tag{13b}$$

$$C_{T2} = \frac{C_{\rm RX} C_m}{C_{\rm sum}} \tag{13c}$$

where

$$\frac{1}{C_{\rm sum}} = \frac{1}{C_{\rm TX}} + \frac{1}{C_m} + \frac{1}{C_{\rm RX}}. \tag{14}$$

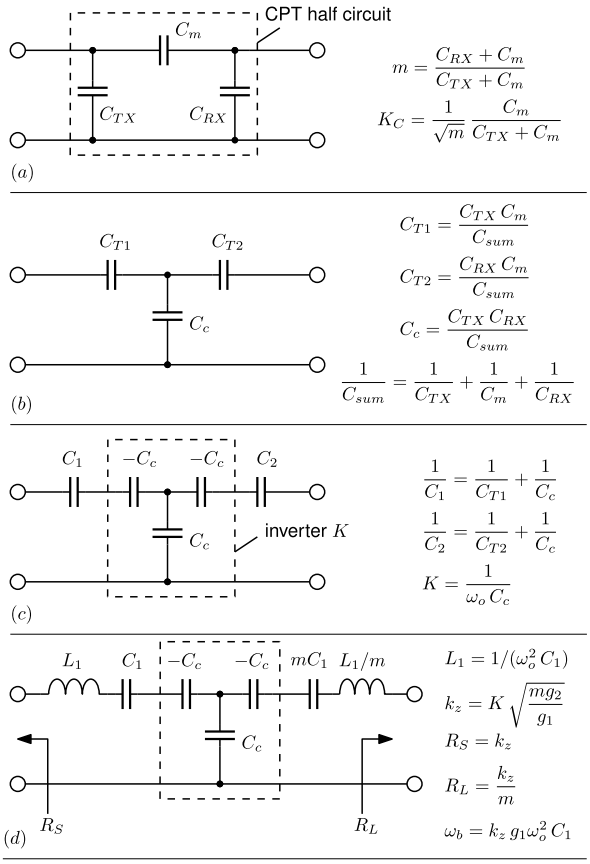

Fig. 4. Summary of steps to transform an equivalent CPT half circuit into a filter prototype with matched ports: (a) half-circuit; (b) equivalent half-circuit as a T-network; (c) partitioning circuit to include an impedance inverter; and (d) circuit with matching inductors to realize a bandpass filter.

The equivalent T-network of capacitances is shown in Fig. 4(b).

From the theory in Section III, the capacitances C_{T1} and C_{T2} are each partitioned into two series capacitances, one of which is equal to $-C_c$. The partitioned capacitances are shown in Fig. 4(c) where

$$\frac{1}{C_1} = \frac{1}{C_{T1}} + \frac{1}{C_c} \tag{15}$$

and

$$\frac{1}{C_2} = \frac{1}{C_{T2}} + \frac{1}{C_c}. \tag{16}$$

After partitioning, the three capacitors of capacitance $\pm C_c$ can be approximated by an ideal impedance inverter with impedance parameter

$$K = \frac{1}{\omega_o C_c}. \tag{17}$$

In the final step, series matching inductors are added to the capacitance network to complete the design. The final circuit is shown in Fig. 4(d). At this point, we can now use filter theory to complete the design and find values for the matching inductors and port resistances. The equations are given in Fig. 4(d) and expressed in terms of filter prototype constants g_n. The values for g_n are selected for a specific

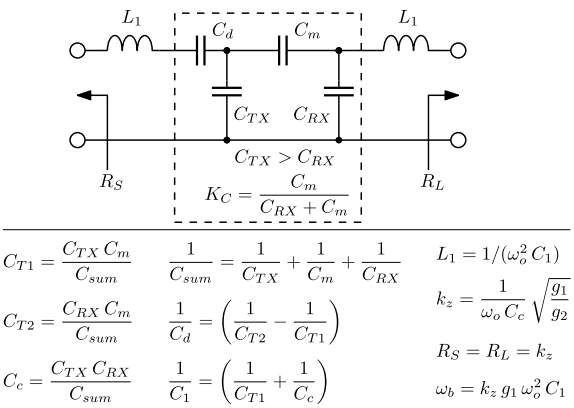

Fig. 5. CPT half circuit with additional series capacitor C_d to equalize the port resistances such that $R_S = R_L$.

type of frequency response. For critical coupling, a Butterworth filter prototype is used. For overcoupling, Chebyshev filter prototype values are used. Examples of both types are frequency response characteristics that are given in Section V.

Before considering design examples, a few comments are made about the port resistances in Fig. 4(d). If the CPT link is symmetric, $m = 1$, and we see that the transmit and receive ports have identical termination resistances. On the other hand, if the link is asymmetric, the port resistances for maximum power transfer are unequal. If equal port resistances are required for asymmetric CPT links, we can modify the filter matching network to include a compensating series capacitor. This method is shown in Fig. 5 where it is assumed that $C_{\rm TX} > C_{\rm RX}$. A series capacitance C_d is added to the transmit side such that the overall capacitive network in the dashed box is symmetric and $m = 1$. The value of C_d can be found by referring to the equivalent circuit shown in Fig. 4(c). Capacitance C_d is selected such that the series capacitance of C_1 and C_d is equal to C_2, thereby creating a symmetric filter network. Therefore, we have two options for asymmetric CPT. The first is a design where $R_S \neq R_L$ (see Fig. 4), and the second is a design where $R_S = R_L$ (see Fig. 5).

V. Design Examples

We now work through a number of different design examples using the filter theory to design CPT links.

Electrostatic simulations of different physical CPT plate geometries are made using the COMSOL Multiphysics finite-element solver [34]. The Maxwell capacitance matrices are extracted, transformed into equivalent half circuits, and related to the Π-network capacitances $C_{\rm TX}$, $C_{\rm RX}$, and C_m. The geometric parameters are swept, and the closed-form analytic equations are used to compute the corresponding port impedances and matching component values. In this way, a requirement for a specific terminal impedance is related to the geometry of the CPT link.

In each example, we consider two-plate image models of four-plate CPT configurations in Fig. 1(a). Square transmit and receive plates are used for all the designs. The width of the transmit plate is w_1 and the width of the receive plate is w_2, where the transmit plate has the larger plate dimension. In the half-circuit geometry, the transmit plate is orthogonal

TABLE I

BUTTERWORTH FILTER (BW4): $f_o = 13.56$ MHz AND $\Delta = 0.04$

Design Step	Parameter	Value	Parameter	Value
TX geometry	w_1	11 cm	ℓ_1	2 cm
RX geometry	w_2	11 cm	ℓ_2	2 cm
Gap	g	23 cm		
Π Half Circuit	C_{TX}	6.37 pF	C_{RX}	6.37 pF
	C_m	0.18 pF	K_C	0.028
T-network	C_{T1}	6.8 pF	C_{T2}	6.8 pF
	C_c	234.7 pF	K	50 Ω
Filter	m	1	k_z	50 Ω
	R_S	50 Ω	R_L	50 Ω
	L_1	20.7 uH	L_2	20.7 uH

TABLE II

BUTTERWORTH FILTER (BW8): $f_o = 13.56$ MHz AND $\Delta = 0.08$

Design Step	Parameter	Value	Parameter	Value
TX geometry	w_1	18.5 cm	ℓ_1	1 cm
RX geometry	w_2	18.5 cm	ℓ_2	1 cm
Gap	g	23 cm		
Π Half Circuit	C_{TX}	12.67 pF	C_{RX}	12.6 pF
	C_m	0.76 pF	K_C	0.056
T-network	C_{T1}	14.1 pF	C_{T2}	14.1 pF
	C_c	234.7 pF	K	50 Ω
Filter	m	1	k_z	50 Ω
	R_S	50 Ω	R_L	50 Ω
	L_1	10.4 uH	L_2	10.4 uH

to the ground plane with a gap ℓ_1, as shown in Fig. 1(b). Similarly, the receive plate is orthogonal to the ground plane with a gap ℓ_2.

A. Butterworth Filter Examples: Critically Coupled CPT

Three CPT circuit examples are designed with Butterworth filter frequency response characteristics. The examples are all designed for a center frequency of 13.56 MHz with different plate geometries and different fractional bandwidths. The first example, called BW4, is a symmetric CPT link operating over a 4% bandwidth with square plates of side length $w_1 = w_2 = 11$ cm. The second example, called BW8, is a symmetric CPT link operating over an 8% bandwidth with square plates of side length $w_1 = w_2 = 18.5$ cm. For both BW4 and BW8, the distance between the transmit and receive plates g is 23 cm. The larger bandwidth of BW8 can be attributed to the larger plate size used in BW8. This leads to a larger coupling coefficient, which is directly proportional to bandwidth. The third example, called ABW4, is an asymmetric design operating over a 4% bandwidth with square transmit plates of side length 18.5 cm and square receive plates of side length 11 cm. Although the relative bandwidth of ABW4 is the same as BW4, the corresponding gap width is slightly larger, spanning a distance of 26 cm. The asymmetric design also results in unequal terminal impedances when the ports are matched using inductors alone. The three designs are summarized in Tables I–III.

In order to synthesize these designs, we need the equivalent half-circuit capacitances (C_{TX}, C_m, and C_{RX}) and the

TABLE III

BUTTERWORTH FILTER (ABW4): $f_o = 13.56$ MHz AND $\Delta = 0.04$

Design Step	Parameter	Value	Parameter	Value
TX geometry	w_1	18.5 cm	ℓ_1	0.9 cm
RX geometry	w_2	11 cm	ℓ_2	1.8 cm
Gap	g	26 cm		
Π Half Circuit	C_{TX}	13.00 pF	C_{RX}	6.37 pF
	C_m	0.26 pF	K_C	0.028
T-network	C_{T1}	6.8 pF	C_{T2}	6.8 pF
	C_c	332.0 pF	K	34.6 Ω
Filter	m	0.5	k_z	25 Ω
	R_S	25 Ω	R_L	50 Ω
	L_1	10.4 uH	L_2	20.7 uH

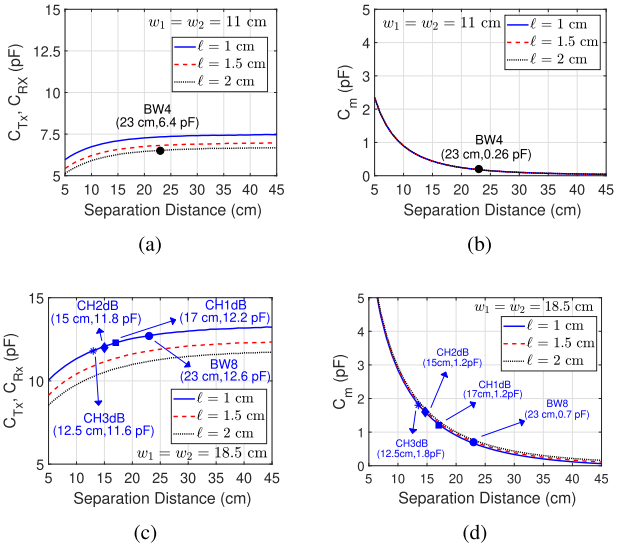

Fig. 6. Equivalent half-circuit capacitances derived from electrostatic simulations of four-plate CPT with symmetric pairs of transmit and receive plates. For plates of side length 11 cm: (a) C_{TX} and C_{RX}; (b) C_m. For plate side length 18.5 cm: (c) C_{TX} and C_{RX}; (d) C_m. Specific points are labeled that correspond to design examples. CPT links with Butterworth filter frequency response characteristics are labeled as BW4 (4% relative bandwidth) and BW8 (8% relative bandwidth). CPT links with Chebyshev characteristics are labeled as CH1dB (1 dB ripple), CH2dB (2 dB ripple), and CH3dB (3 dB ripple). The capacitances are shown as a function of the distance between the transmit and receive plates and parameterized for different heights relative to the virtual ground plane.

filter coefficients g_n. All three Butterworth filter designs are derived from a canonical second -order filter prototype with coefficients

$$g_0 = 1, \quad g_1 = 1.4142, \; g_2 = 1.4142, \; g_3 = 1. \qquad (18)$$

The equations in Fig. 4 are used to determine the terminal impedances (R_S and R_L) and the matching inductors (L_1 and L_2).

Electrostatic simulations are performed in COMSOL to find the equivalent half-circuit capacitances. These capacitance values are shown in Fig. 6 for symmetric transmit and receive plates. The half-circuit capacitances are used to calculate the terminal resistances and inductor values. By combining the analytic equations with geometric sweeps in COMSOL, plots are generated to show how the matching inductance, terminal resistance, and relative frequency bandwidth change with geometric parameters. Examples of these plots are shown

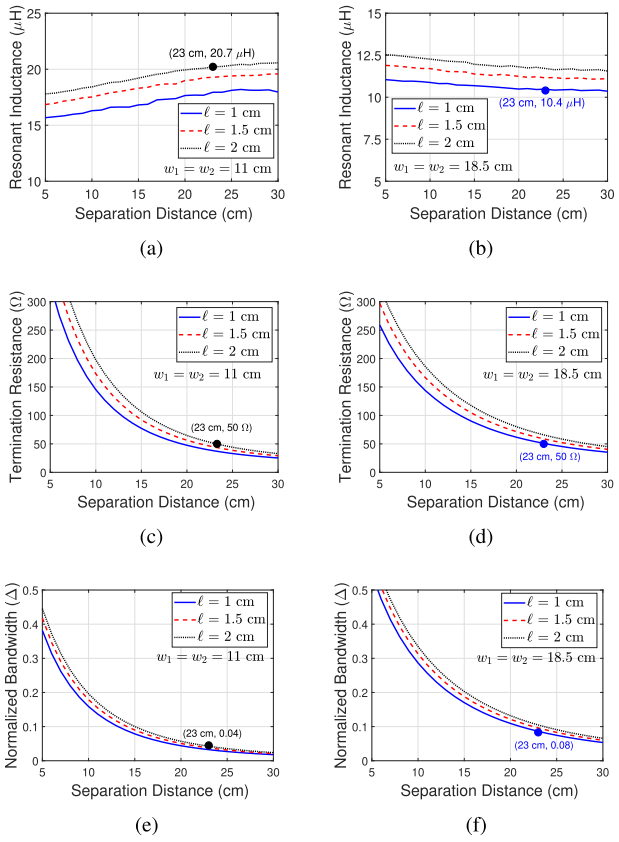

Fig. 7. Relationship between matching inductance, port termination resistance, and normalized frequency bandwidth is plotted versus geometric parameters. (a), (c), and (e) BW4. (b), (d), and (f) BW8.

in Fig. 7 for designs BW4 and BW8. Both filters are designed for a gap of 23 cm and the port resistances of 50 Ω.

B. Chebychev Filter Examples: Overcoupled CPT

When the coupling coefficient exceeds critical coupling, the CPT link is overcoupled. For a two-resonator system, the overcoupled frequency response has two peaks with a dip at the center frequency. This response is modeled by a second-order bandpass filter with a Chebyshev frequency response. The ripple in the passband determines how much attenuation the overcoupled response has at the center frequency of the filter. Fundamentally, the passband ripple in a Chebyshev filter arises through impedance mismatch and a design can be constructed for a specified ripple. Three examples are discussed next where the ripple (ε) values are varied from 1 to 3 dB.

The coefficients (g_n) for three different second-order Chebychev filter prototypes are given in Table IV. The filter coefficients are used in conjunction with the equivalent half-circuit capacitances to design three different CPT links. The designs are summarized in Tables V–VII.

Since the typical operation of a CPT link has spatial variation that modifies the coupling between the transmitter and the receiver, the Chebyshev filter designs were selected to provide a comparison with one of the critically coupled designs described in Section V-A. The Butterworth filter with 8% relative bandwidth (BW8) was used as a reference for the critical-coupled condition, and the gap g between the transmitter and the receiver is reduced to create an overcoupled condition. The gap for critical coupling is 23 cm for 18.5-cm square plates placed 1 cm above the virtual ground plane (see Table II). We decided to use the geometry of BW8 as a constraint for the Chebyshev filter designs with

TABLE IV
CHEBYCHEV FILTER COEFFICIENTS

ε (dB)	g_0	g_1	g_2	g_3
1	1	1.8289	0.6850	2.6599
2	1	2.4881	0.6075	4.0957
3	1	3.1013	0.5339	5.8095

TABLE V
CHEBYCHEV FILTER (CH1DB): $f_o = 13.56$ MHz, $\varepsilon = 1$ dB, AND $\Delta = 0.103$

Design Step	Parameter	Value	Parameter	Value
TX geometry	w_1	18.5 cm	ℓ_1	1 cm
RX geometry	w_2	18.5 cm	ℓ_2	1 cm
Gap	g	17 cm		
Π Half Circuit	C_{TX}	12.16 pF	C_{RX}	12.16 pF
	C_m	1.23 pF	K_C	0.092
T-network	C_{T1}	14.6 pF	C_{T2}	14.6 pF
	C_c	144.0 pF	K	81.5 Ω
Filter	m	1	k_z	50 Ω
	R_S	50 Ω	R_L	50 Ω
	L_1	10.4 uH	L_2	10.4 uH

TABLE VI
CHEBYCHEV FILTER (CH2DB): $f_o = 13.56$ MHz, $\varepsilon = 2$ dB, AND $\Delta = 0.14$

Design Step	Parameter	Value	Parameter	Value
TX geometry	w_1	18.5 cm	ℓ_1	1 cm
RX geometry	w_2	18.5 cm	ℓ_2	1 cm
Gap	g	15 cm		
Π Half Circuit	C_{TX}	11.86 pF	C_{RX}	11.86 pF
	C_m	1.52 pF	K_C	0.112
T-network	C_{T1}	14.9 pF	C_{T2}	14.9 pF
	C_c	116.0 pF	K	120.5 Ω
Filter	m	1	k_z	50 Ω
	R_S	50 Ω	R_L	50 Ω
	L_1	10.4 uH	L_2	10.4 uH

TABLE VII
CHEBYCHEV FILTER (CH3DB): $f_o = 13.56$ MHz, $\varepsilon = 3$ dB, AND $\Delta = 0.176$

Design Step	Parameter	Value	Parameter	Value
TX geometry	w_1	18.5 cm	ℓ_1	1 cm
RX geometry	w_2	18.5 cm	ℓ_2	1 cm
Gap	g	12.5 cm		
Π Half Circuit	C_{TX}	11.72 pF	C_{RX}	11.72 pF
	C_m	1.86 pF	K_C	0.137
T-network	C_{T1}	15.4 pF	C_{T2}	15.4 pF
	C_c	97.4 pF	K	120.5 Ω
Filter	m	1	k_z	50 Ω
	R_S	50 Ω	R_L	50 Ω
	L_1	10.4 uH	L_2	10.4 uH

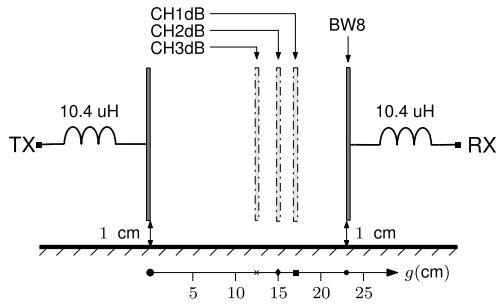

g (cm)	Filter	Attenuation at f_o (dB)	Δ	k_c
23	BW8	0	0.08	0.056
17	CH1dB	1	0.10	0.092
15	CH2dB	2	0.14	0.112
12.5	CH3dB	3	0.18	0.137

(a)

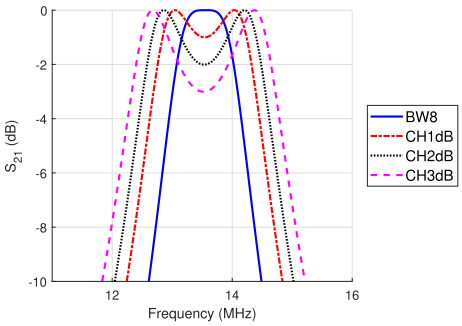

(b)

Fig. 8. Frequency response of a CPT link for different transmission gap distances. (a) Physical configuration and (b) Corresponding frequency response.

the additional requirement that the matching inductors also remain unchanged. Therefore, in all the Chebyshev designs, $L_1 = L_2 = 10.4\ \mu$H, the same as BW8. Therefore, the plate geometry and matching components for the Chebyshev designs are constrained and the only variable is the distance between the transmit and receive plates. The distance is adjusted to change the amount of overcoupling in the frequency response. As shown in the design tables, at a distance of 23 cm, the CPT is critically coupled (BW8); at 17 cm, the CPT is overcoupled with a 1-dB dip at f_o (CH1dB); at 15 cm, the CPT is overcoupled with a 2-dB dip at f_o (CH2dB); and at 12.5 cm, the CPT is overcoupled with a 3-dB dip at f_o (CH3dB). The relationships between the gap distance and the frequency response are summarized in Fig. 8.

C. Frequency and Spatial Bandwidths

An interesting question, which comes from connecting filter theory with WPT applications, is whether there are connections between the frequency and spatial bandwidths. Fundamentally, whether we measure bandwidth in terms of a frequency changes or in terms of a spatial changes, the attenuation in power transfer is related to an impedance change in the circuit. Attenuation is the result of an impedance mismatch. Therefore, if the -3 dB bandwidth is a measure of interest, this corresponds to a power transfer efficiency of 50%

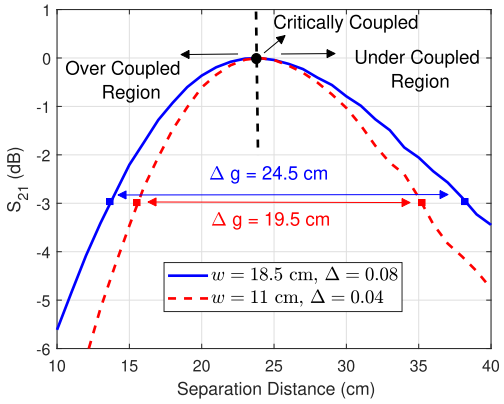

Fig. 9. This plot shows how the magnitude of the transmission coefficient S_{21} changes as a function of the gap distance between the transmitter and the receiver. Responses are shown for two different Butterworth filter designs: BW4 and BW8. The -3-dB spatial bandwidth (Δg) is shown for both designs. The correlation between the frequency and spatial bandwidths is evident: BW8 has a larger relative bandwidth (0.08) and a larger spatial bandwidth (24.5 cm) compared with BW4 that has a relative bandwidth of 0.04 and a spatial bandwidth of 19.5 cm.

across the link or an impedance mismatch with a reflection coefficient of $1/\sqrt{2} \approx 0.7$. The impedance mismatch is created by either changing frequency, as in the case of a filter, or by changing the spatial configuration as in the case of a CPT link.

We can use the examples to gain some insight into the relationship between the frequency and spatial bandwidths. The Butterworth filters BW4 and BW8 have normalized frequency bandwidths (Δ) of 0.04 and 0.08, respectively. Both filters are designed to have critical coupling for a gap of 23 cm. Therefore, they are good candidates for comparing the spatial bandwidth of two different designs that have two different frequency bandwidths: BW8 has twice the bandwidth of BW4.

The spatial bandwidths of BW4 and BW8 are measured by varying the gap distance between the transmitter and the receiver. No changes are made to plate geometry or the matching inductors. The results are shown in Fig. 9. For the filter with a relative frequency bandwidth of 0.04, the -3-dB spatial bandwidth (Δg) is 19.5 cm. These results are compared with BW8, which has a wider frequency bandwidth, where we see that the spatial bandwidth is also wider by 26.5%.

The correlation between the frequency and spatial bandwidths is expected because of the relationship in (12), which shows that the coupling coefficient K_C is equal to $\Delta/(g_1\, g_2)^{1/2}$. The coupling coefficient is in turn derived from the capacitances in the half-circuit model, as shown in (12). However, since spatial changes in capacitance are nonlinear (see Fig. 6), the relationship between the frequency and spatial bandwidths is nonlinear. Although the correlation between the frequency and spatial bandwidths is nonlinear, we can use this correlation to guide the design of matching circuits where we expect that a matching circuit with wider bandwidth will lead to an improvement in spatial bandwidth.

D. Filter Losses

The filter theory described so far has focused on minimizing CPT mismatch losses over a range of frequencies, assuming

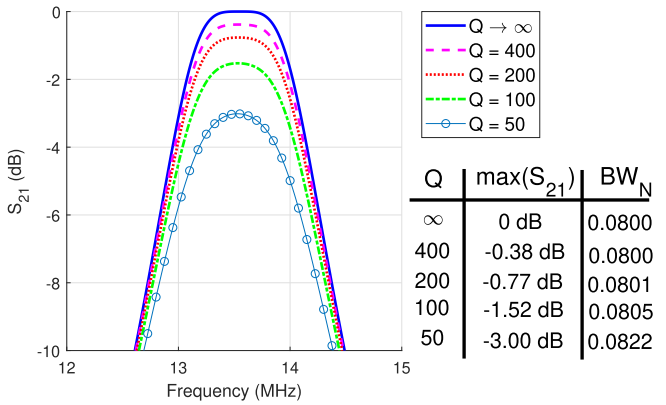

Q	max(S_{21})	BW_N
∞	0 dB	0.0800
400	-0.38 dB	0.0800
200	-0.77 dB	0.0801
100	-1.52 dB	0.0805
50	-3.00 dB	0.0822

Fig. 10. Frequency response of BW8 ($K_C = 0.056$) for different values of inductor Q. The transmission efficiency (dB) as well as normalized bandwidth (BW_N) are shown in the figure. The simulated efficiencies match with values calculated using (19).The bandwidth of the filter response does not change significantly and varies by 2.75% as Q is changed from infinity to 50.

that all network components are ideal. Once impedance is optimized, the efficiency of the CPT is ultimately determined by the quality factor of the components in the network. If finite resonator Q is accounted for, the efficiency of a two resonator CPT link can be expressed as

$$\eta = \frac{K_C^2\, Q_1\, Q_2}{\left[1 + \sqrt{1 + K_C^2\, Q_1\, Q_2}\right]^2} \tag{19}$$

where Q_1 and Q_2 are the unloaded quality factors of the transmitter- and receiver-side resonators [24].

The impact of loss in filter design has been investigated for various loss mechanisms [32], [35], [36]. Here, we examine the impact of inductor loss through simulation and show that the simulated transmission efficiency is consistent with (19). Fig. 10 shows the filter response for a maximally flat filter (BW8) for different values of inductor Q. The filter is symmetric and the matching inductors are assumed to have the same Q ($Q_1 = Q_2$). The plot shows that providing that Q is greater than 50, the overall shape of the frequency response does not change significantly. For Q of 50, the normalized bandwidth changes by 2.75% compared with the ideal response. Under these conditions, the primary effect of loss is an increase in attenuation in the S_{21} response. Therefore, the insertion loss at midband reduces the overall efficiency of the CPT link. The transmission efficiencies of the simulation results in Fig. 10 are identical to results obtained using (19). For example, with Q of 50 and K_C of 0.056, the calculated efficiency is 50%, which corresponds to a -3 dB transmission efficiency.

VI. Experimental Verification

Experimental prototypes of the six filter examples (BW4, BW8, ABW8, CH1dB, CH2dB, and CH3dB) were built to verify the filter design methodology. Equivalent two-plate systems were constructed to implement image configurations of four-plate CPT configurations. In this way, the experimental results could be compared directly with analytic and simulation results. Furthermore, an advantage of the two-plate geometry is that measurements could be easily carried out using a vector network analyzer without the need for additional baluns.

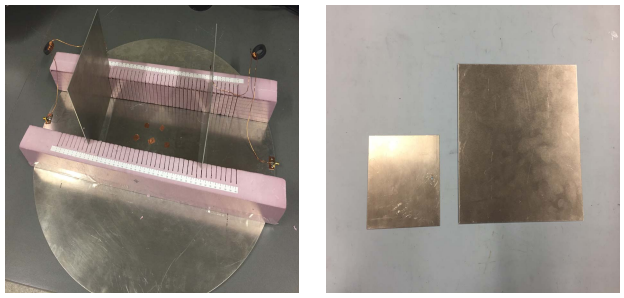

(a) (b)

Fig. 11. Experimental setup for measuring the CPT half-circuit filter responses. (a) Test bed. (b) Example of the aluminum plates used for implementing the CPT link. The plate on the left is 11 cm × 11 cm and the plate on the right is 18.5 cm × 18.5 cm.

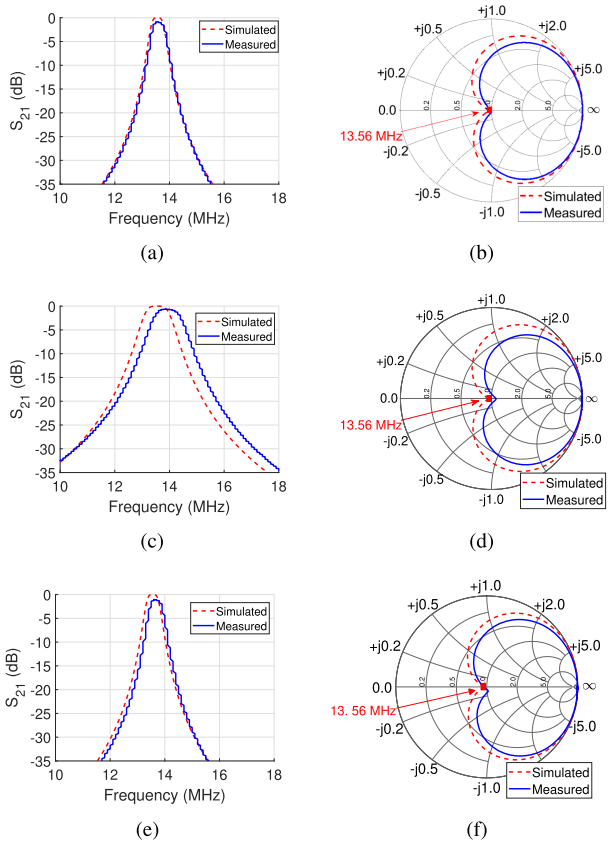

(a) (b) (c) (d) (e) (f)

Fig. 12. Measurement results are shown for the CPT half circuits with Butterworth frequency response characteristics. (a) Transmission response for BW4. (b) Input impedance of BW4. (c) Transmission response for BW8. (d) Input impedance of BW8. (e) Transmission response of the asymmetric filter ABW4. (f) Input impedance of ABW4. The filter insertion loss is −0.85 dB for BW4, −0.54 dB for BW8, and −1.06 dB for ABW4. Measurements for ABW4 include a 2:1 output balun at the transmit port to transform the port impedance to 50 Ω.

The plates were constructed out of aluminum and mounted in polystyrene holders. The plates were placed on a ground plane and the height above the ground plane was adjusted to match the design values for ℓ_1 and ℓ_2. SMA connectors are attached to the ground plate and connected in series with matching inductors to the transmit and receive plates. A photograph of the measurement setup is shown in Fig. 11.

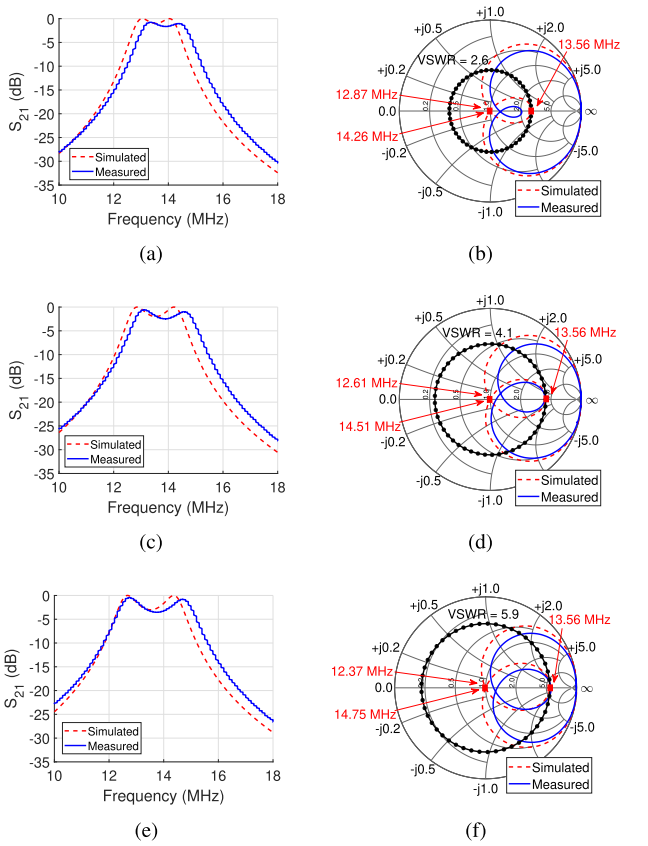

Fig. 13. Measurement results are shown for the CPT half circuits with Chebyshev (overcoupled) frequency response characteristics. (a) Transmission response for CH1dB. (b) Input impedance of CH1dB. (c) Transmission response for CH2dB. (d) Input impedance of CH2dB. (e) Transmission response of the asymmetric filter CH3dB. (f) Input impedance of CH3dB. Note the ripple level and bandwidth differences between the filter designs. The measured insertion loss is −0.54, −0.48, and −0.43 dB for designs with the ripple level of 1, 2, and 3 dB, respectively.

Matching inductors were wound on ferrite cores made of material 67 from Fair-Rite Products Corporation [37]. Material 67 is a high-frequency NiZn ferrite that can be used to implement high Q inductors up to 50 MHz. The relative permeability of the core material is 40, and the loss tangent of the material is 0.0048. Cores with an inner diameter of 19.05 mm and an outer diameter of 31.75 mm were used. The manufacturer specification for the inductance factor (A_L) is 39 nH per wire-turn squared.

Four of the filter designs (BW8, CH1dB, CH2dB, and CH3dB) require 10.4-μH inductors, and two of the designs require 20.7 μH inductors (BW4 and ABW8). Both inductor values were made using AWG 16 gauge tin-coated copper wire. Thirteen turns were used for the 10.4-μH inductor and twenty turns were used for the 20.7-μH inductor.

Each filter circuit was spatially configured to match the designs tabulated in Section V. The filter frequency responses (S_{21}) and the input matches (S_{11}) were measured with a Copper Mountain Technologies Planar 304/1 3.2-GHz vector network analyzer with an input power of 10 dBm. The measurement results for BW4, BW8, and ABW8 are shown in Fig. 12, and the measurement results for CH1dB, CH2dB, and CH3dB are shown in Fig. 13. The figures also include the simulation results for comparison.

Overall, the experimental results confirm the filter design theory that was used to implement the CPT half circuits. The results show good agreement with theory in terms of relative bandwidth and in-band ripple for the overcoupled Chebyshev filters. The most significant discrepancy between the measurement and simulation results is the insertion loss of the filters. For BW4 and BW8, the minimum insertion loss is approximately 0.54 and 0.85 dB, which is attributed to the finite Q of the inductors. For the asymmetric filter ABW4 in Fig. 12, the insertion loss is 1.06 dB, which includes the loss of a 2:1 balun on the transmit port to transform the 25-Ω port impedance to 50-Ω. Exact measurements for each filter are reported in the figure captions. Since the primary objective of the experimental measurements was to verify the theory presented in this article, further work to improve inductor Q was not pursued. For examples of low-loss inductor design, the reader is referred to other papers [38].

VII. Conclusion

In this article, we have used the filter theory to analyze the coupling, matching, and termination resistances in a CPT link. Reformulating CPT systems in the context of filter theory enables designers to quickly determine the geometry and matching networks required to achieve an optimal frequency response. In our approach to CPT design, we begin with a specific plate geometry that needs to be scaled and sized to efficiently deliver power over a gap between the transmitter and the receiver. The physical dimensions ultimately lead to electrical constraints that include the size of matching inductors and the optimum load resistances that lead to maximum power transfer. For a CPT link with a stationary transmitter and receiver, we can design a link that is critically coupled, which has a maximally flat frequency response. For CPT links where the transmitter and receiver are not stationary, the system needs to be robust to spatial misalignment and the spatial bandwidth of the system becomes important. With fixed matching elements, any spatial variations within the link will modify the coupling and operation under overcoupled (Chebyshev frequency response) and undercoupled conditions need to be considered in addition to critical coupling (Butterworth frequency response).

In Section III, we began with a canonical bandpass filter prototype and transformed the circuit into an equivalent half circuit that is composed of a Π-network of capacitances that model plate capacitances and matching inductors. An important step in transforming the filter structure, and a step that makes it useful for CPT, is to recognize that the coupling in CPT can be modeled using impedance inverters. An important point highlighted by the analysis is that the impedance of the inverter is implicitly determined by plate geometry. This relation is captured in (17) and shows how the impedance parameter K depends on the capacitance C_c, which is determined by the plate capacitances. The inverter impedance directly controls the optimum load resistance through the impedance scaling parameter k_z. This shows how the terminal resistances are intrinsically related to the physical geometry of the plates. We can, therefore, optimize plate geometry for specific terminal resistances using filter design equations.

The filter model also includes networks that match the capacitor Π-network to the port resistances. The matching inductors appear naturally from the canonical filter prototype circuits. The filter theory can also be used to customize the matching for a specific frequency response. If we want to match for critical coupling, we can determine the matching inductors and optimum port impedances using the Butterworth prototypes. If instead, we want to match for a specific level of overcoupling, we can determine the matching inductors and optimum port impedances using the Chebyshev prototypes.

Six design examples of different CPT half circuits were shown to illustrate the filter design methodology. The examples included two different symmetric CPT configurations (i.e., with the same transmit and receive plate sizes) matched for critical coupling. From these two examples, we also investigated relationships between the spatial and frequency bandwidths, where we observed that the design with the larger frequency bandwidth also had a larger spatial bandwidth. This provided evidence that broadband frequency matching could be advantageous in terms of improving spatial robustness in CPT. Another example illustrated a critically coupled asymmetric link, which resulted in unequal optimum load and source resistances. This showed how asymmetry could be used to transform impedance between the transmitter and the receiver.

Three examples of Chebyshev filter matching circuits were also shown to illustrate overcoupled responses. The overcoupled analysis using the Chebyshev filters provides insight into attenuation at midband for spatial changes. The analytic equations can also be used to determine how port resistance modifies the overcoupled response. These examples show how filter theory techniques can be used to analyze and design CPT wireless coupling, and we expect that new insights will be found as the connections between filters and wireless power systems continue to be explored.

ACKNOWLEDGMENT

The authors acknowledge CMC Microsystems for the provision of CAD tools that facilitated this research.

REFERENCES

[1] G. A. Peek, M. R. Francis, and T. W. Frank, "Wireless charging device for wearable electronic device," U.S. Patent 9 843 214, Dec. 12, 2017.

[2] L. Huang and A. P. Hu, "Defining the mutual coupling of capacitive power transfer for wireless power transfer," *Electron. Lett.*, vol. 51, no. 22, pp. 1806–1807, Oct. 2015.

[3] A. K. Ramrakhyani, S. Mirabbasi, and M. Chiao, "Design and optimization of resonance-based efficient wireless power delivery systems for biomedical implants," *IEEE Trans. Biomed. Circuits Syst.*, vol. 5, no. 1, pp. 48–63, Feb. 2011.

[4] L. Xie, Y. Shi, Y. T. Hou, and H. D. Sherali, "Making sensor networks immortal: An energy-renewal approach with wireless power transfer," *IEEE/ACM Trans. Netw.*, vol. 20, no. 6, pp. 1748–1761, Dec. 2012.

[5] J. M. Miller, P. H. Chambon, P. T. Jones, and C. P. White, "Wireless power transfer electric vehicle supply equipment installation and validation tool," U.S. Patent 13 544 058, Jan. 24, 2013.

[6] A. Ahmad, M. S. Alam, and R. Chabaan, "A comprehensive review of wireless charging technologies for electric vehicles," *IEEE Trans. Transport. Electrific.*, vol. 4, no. 1, pp. 38–63, Mar. 2018.

[7] S. Sinha, A. Kumar, B. Regensburger, and K. K. Afridi, "A new design approach to mitigating the effect of parasitics in capacitive wireless power transfer systems for electric vehicle charging," *IEEE Trans. Transport. Electrific.*, vol. 5, no. 4, pp. 1040–1059, Dec. 2019.

[8] A. Kurs, A. Karalis, R. Moffatt, J. D. Joannopoulos, P. Fisher, and M. Soljacic, "Wireless power transfer via strongly coupled magnetic resonances," *Science*, vol. 317, no. 5834, pp. 83–86, Jul. 2007.

[9] M. Kline, I. Izyumin, B. Boser, and S. Sanders, "Capacitive power transfer for contactless charging," in *Proc. 26th Annu. IEEE Appl. Power Electron. Conf. Expo. (APEC)*, Mar. 2011, pp. 1398–1404.

[10] S. H. Jeong, E. T. Ozaki, L. S. Irish, and W. H. Von Novak, III, "Inductive and capacitive wireless power transfer," U.S. Patent 14 838 404, Mar. 2, 2017.

[11] J. Kim, D.-H. Kim, and Y.-J. Park, "Analysis of capacitive impedance matching networks for simultaneous wireless power transfer to multiple devices," *IEEE Trans. Ind. Electron.*, vol. 62, no. 5, pp. 2807–2813, May 2015.

[12] B. Regensburger *et al.*, "High-performance large air-gap capacitive wireless power transfer system for electric vehicle charging," in *Proc. IEEE Transp. Electrific. Conf. Expo (ITEC)*, Jun. 2017, pp. 638–643.

[13] B. Regensburger, J. Estrada, A. Kumar, S. Sinha, Z. Popovic, and K. K. Afridi, "High-performance capacitive wireless power transfer system for electric vehicle charging with enhanced coupling plate design," in *Proc. IEEE Energy Convers. Congr. Expo. (ECCE)*, Sep. 2018, pp. 2472–2477.

[14] W. Zhang and C. C. Mi, "Compensation topologies of high-power wireless power transfer systems," *IEEE Trans. Veh. Technol.*, vol. 65, no. 6, pp. 4768–4778, Jun. 2016.

[15] Y. Chen *et al.*, "Variable-parameter T-circuit-based IPT system charging battery with constant current or constant voltage output," *IEEE Trans. Power Electron.*, vol. 35, no. 2, pp. 1672–1684, Feb. 2020.

[16] N. Keeling, G. A. Covic, F. Hao, L. George, and J. T. Boys, "Variable tuning in LCL compensated contactless power transfer pickups," in *Proc. IEEE Energy Convers. Congr. Expo.*, Sep. 2009, pp. 1826–1832.

[17] J. Lee, Y.-S. Lim, W.-J. Yang, and S.-O. Lim, "Wireless power transfer system adaptive to change in coil separation," *IEEE Trans. Antennas Propag.*, vol. 62, no. 2, pp. 889–897, Feb. 2014.

[18] J. Lee, Y. Lim, H. Ahn, J.-D. Yu, and S.-O. Lim, "Impedance-matched wireless power transfer systems using an arbitrary number of coils with flexible coil positioning," *IEEE Antennas Wireless Propag. Lett.*, vol. 13, pp. 1207–1210, 2014.

[19] L. Huang, A. P. Hu, A. K. Swain, and Y. Su, "Z-impedance compensation for wireless power transfer based on electric field," *IEEE Trans. Power Electron.*, vol. 31, no. 11, pp. 7556–7563, Nov. 2016.

[20] S. Sinha, A. Kumar, S. Pervaiz, B. Regensburger, and K. K. Afridi, "Design of efficient matching networks for capacitive wireless power transfer systems," in *Proc. IEEE 17th Workshop Control Modeling Power Electron. (COMPEL)*, Jun. 2016, pp. 1–7.

[21] F. Lu, H. Zhang, H. Hofmann, and C. C. Mi, "A double-sided LC-compensation circuit for loosely coupled capacitive power transfer," *IEEE Trans. Power Electron.*, vol. 33, no. 2, pp. 1633–1643, Feb. 2018.

[22] S. Wenngren, A. Clements, and T. Johnson, "Capacitively coupled resonator models for investigating spatial impedance variation in WPT systems," in *Proc. IEEE Wireless Power Transf. Conf. (WPTC)*, Jun. 2018, pp. 1–4.

[23] S. E. Wenngren, "Analysis and design of capacitively coupled resonators for wireless power transfer system applications," M.S. thesis, School Eng., Univ. British Columbia, Kelowna, BC, Canada, 2019.

[24] T. Komaru and H. Akita, "Positional characteristics of capacitive power transfer as a resonance coupling system," in *Proc. IEEE Wireless Power Transf. (WPT)*, May 2013, pp. 218–221.

[25] C. Liu, A. P. Hu, and M. Budhia, "A generalized coupling model for capacitive power transfer systems," in *Proc. IECON-36th Annu. Conf. IEEE Ind. Electron. Soc.*, Nov. 2010, pp. 274–279.

[26] L. Huang, A. P. Hu, A. K. Swain, and Y. Su, "Accurate steady-state modeling of capacitive-coupling interface of capacitive power transfer systems with cross-coupling," *Wireless Power Transf.*, vol. 3, no. 1, pp. 53–62, Mar. 2016.

[27] F. Lu, H. Zhang, H. Hofmann, and C. Mi, "A CLLC-compensated high power and large air-gap capacitive power transfer system for electric vehicle charging applications," in *Proc. IEEE Appl. Power Electron. Conf. Expo. (APEC)*, Mar. 2016, pp. 1721–1725.

[28] H. Zhang, F. Lu, H. Hofmann, W. Liu, and C. C. Mi, "Six-plate capacitive coupler to reduce electric field emission in large air-gap capacitive power transfer," *IEEE Trans. Power Electron.*, vol. 33, no. 1, pp. 665–675, Jan. 2018, doi: 10.1109/TPEL.2017.2662583.

[29] C. A. Balanis, *Antenna Theory: Analysis and Design*, 4th ed. New York, NY, USA: Wiley, 2016.

[30] E. A. Guillemin, *Synthesis of Passive Networks: Theory and Methods Appropriate to the Realization and Approximation Problems*. Hoboken, NJ, USA: Wiley, 1957.
[31] G. Matthaei, L. Young, and E. Jones, "Design of microwave filters, impedance-matching networks, and coupling structures: Volume 1," Stanford Res. Inst., Menlo Park, CA, USA, Tech. Rep. 3527, 1963.
[32] A. Zverev, *Handbook of Filter Synthesis*, 1st ed. New York, NY, USA: Wiley, 1967.
[33] R. E. Collin, *Foundations for Microwave Engineering*, 2nd ed. New York, NY, USA: Wiley, 2007.
[34] COMSOL AB, Stockholm, Sweden. (2018). *COMSOL Multiphysics*. [Online]. Available: https://www.comsol.com
[35] C.-M. Tsai and H.-M. Lee, "The effects of component Q distribution on microwave filters," *IEEE Trans. Microw. Theory Techn.*, vol. 54, no. 4, pp. 1545–1553, Jun. 2006.
[36] M. Oldoni, G. Macchiarella, G. G. Gentili, and C. Ernst, "A new approach to the synthesis of microwave lossy filters," *IEEE Trans. Microw. Theory Techn.*, vol. 58, no. 5, pp. 1222–1229, May 2010.
[37] Fair-Rite. *Toroids, Datasheet 5967001701*. Accessed: Aug. 2, 2019. [Online]. Available: https://www.fair-rite.com/product_datasheet/PN5967001701.html
[38] K. Doubleday, A. Kumar, S. Sinha, B. Regensburger, S. Pervaiz, and K. Afridi, "Design tradeoffs in a multi-modular capacitive wireless power transfer system," in *Proc. IEEE PELS Workshop Emerg. Technol., Wireless Power Transf. (WoW)*, Oct. 2016, pp. 35–41.

Masoud Ahmadi (Student Member, IEEE) received the M.A.Sc. degree in electrical engineering from The University of British Columbia, Kelowna, BC, Canada, with a focus on applied electromagnetics, in 2018, where he is currently pursuing the Ph.D. degree with a focus on wireless solutions for power transmission.

Loïc Markley (Senior Member, IEEE) received the B.A.Sc. degree in electronics engineering from Simon Fraser University, Burnaby, BC, Canada, in 2004, and the M.A.Sc. and Ph.D. degrees in electrical engineering from the University of Toronto, Toronto, ON, Canada, in 2007 and 2013, respectively.

He is currently an Assistant Professor with the School of Engineering, The University of British Columbia, Kelowna, BC, Canada. His research interests include applied electromagnetics, artificial dielectrics and metamaterials, transmission-line structures, passive microwave circuits, frequency-selective surfaces, leaky-wave antennas, and wireless power transfer.

Dr. Markley was a recipient of the Tatsuo Itoh Best Paper Award for his paper on near-field focusing published in the IEEE MICROWAVE AND WIRELESS COMPONENTS LETTERS in 2010. He has been serving as an Associate Editor for the IEEE ANTENNAS AND WIRELESS PROPAGATION LETTERS since 2015.

Thomas Johnson (Member, IEEE) received the B.A.Sc. degree in electrical engineering from The University of British Columbia (UBC), Vancouver, BC, Canada, in 1987, and the M.A.Sc. and Ph.D. degrees from Simon Fraser University, Burnaby, BC, Canada, in 2001 and 2007, respectively, with a focus on research in RF and microwave power amplifiers.

Before joining UBC in 2009, He worked as a technical lead in a number of high-tech companies, including PulseWave RF, Austin, TX, USA; ADC Telecommunications, Vancouver, BC, Canada; and Norsat International, Vancouver, BC, Canada. He is currently an Associate Professor with the School of Engineering, UBC. His research interests include the design of radio frequency circuits and systems, wireless power systems, wireless sensors, and industrial applications of RF/microwave power.